



# Ore-Forming Fluid Evolution in the Giant Gejiu Sn–Cu Polymetallic Ore Field, SW China: Evidence From Fluid Inclusions

Yongqing Chen<sup>1\*</sup>, Zhenyi Wang<sup>1,2</sup> and Jiande Li<sup>1</sup>

<sup>1</sup>School of Earth Sciences and Resources, China University of Geosciences, Beijing, China, <sup>2</sup>Hohhot Natural Resources Comprehensive Survey Center, China Geological Survey, Hohhot, China

## OPEN ACCESS

### Edited by:

Ryan Mathur,  
Juniata College, United States

### Reviewed by:

John Leslie Walshe,  
Mineral Resources—CSIRO, Australia  
Guoguang Wang,  
Nanjing University, China

### \*Correspondence:

Yongqing Chen  
yqchen@cugb.edu.cn

### Specialty section:

This article was submitted to  
Economic Geology,  
a section of the journal  
Frontiers in Earth Science

**Received:** 19 January 2021

**Accepted:** 28 June 2021

**Published:** 09 July 2021

### Citation:

Chen Y, Wang Z and Li J (2021) Ore-Forming Fluid Evolution in the Giant Gejiu Sn–Cu Polymetallic Ore Field, SW China: Evidence From Fluid Inclusions. *Front. Earth Sci.* 9:655777. doi: 10.3389/feart.2021.655777

The giant Gejiu Sn–Cu polymetallic ore deposit is one of the largest Sn producers in the world, and is related in time and space to highly evolved S type granitic intrusion. The mineralization processes can be divided into four stages: (I) skarnization; (II) greisenization; (III) cassiterite–sulfid; and (IV) cassiterite–tourmaline–quartz. Five types of fluid inclusions were recognized using optical petrography, microthermometry, and Raman spectroscopy. The results of microthermometry revealed the evolution of the ore-forming fluid, from a high temperature with low-to-high salinity to a low temperature with low-to-intermediate salinity. Stage I, skarn Sn–Cu ores were formed by bimetasomatism between the granitic intrusion and the surrounding rock under near-critical conditions with the help of ore-forming fluid. Stage II, the fluid was separated into the coexisting liquid and vapor phases in equilibrium condition, and a large amount of cassiterite–scheelite–beryl–lithium muscovite minerals were formed during greisenization. Stage III, mixing, boiling and immiscibility of different types of fluid solutions took place with a decline in temperature and pressure as well as a change in the Eh–pH, which caused amounts of cassiterites and sulfides to precipitate. Stage IV, stockwork ores characterized by cassiterite–tourmaline–quartz minerals were formed associated with the low temperature and low salinity hydrothermal liquid activity. The laser Raman spectra identified CH<sub>4</sub> in all ore-forming stages, indicating that the ore deposits might have been formed in a relatively reduced environment. CO<sub>2</sub> appeared in all stages in addition to Stage I, and might have been formed due to both immiscibility of fluid solutions with dropping pressure as well as temperature and mixing of different types of fluid solutions. In conclusion, the bimetasomatism, mixing, and immiscibility of fluid solutions should have been responsible for the formation of giant Sn–Cu polymetallic deposits.

**Keywords:** fluid inclusions, ore-forming stages, ore-forming model, Sn–Cu polymetallic deposit, Gejiu ore field, SW China

## INTRODUCTION

The giant Gejiu Sn–Cu polymetallic deposit is located in southeast Yunnan Province, southwest China, which consists of five large deposits—Malage, Songshujiao, Gaosong, Laochang, and Kafang (Figures 1, 2), with approximately 300 Mt of ores with an average grade of 1% Sn and 2% Cu. It also contains 400 Mt of Pb and Zn ores with an average grade of 7% (Pb + Zn). The Sn–Cu polymetallic ore deposits exhibit strong and widespread diversity of alteration and ore types as well as distinct metal zonation centered as granitic intrusion outward: Sn–Cu→Sn–W–Be–Nb–Ta→Sn–Cu→Sn–Pb–Zn–Ag (Mlnlu and Kwak, 1994; Chen et al., 2009; Cheng et al., 2013; Liao et al., 2014). Although it has been suggested that these deposits are genetically associated with Late Cretaceous orogenic granites (308 Geological Party, 1984; Mlnlu and Kwak, 1994; Luo, 1995; Zhuang et al., 1996; Mao et al., 2008; Cheng et al., 2012, 2013; Chen et al., 2020), the ore-forming processes spanning multiple stages remain unclear. Thus, verifying how the components of the ore-forming hydrothermal fluid evolve over time, and how these variations affect the spatial distribution of ore minerals and alteration zones are challenging tasks. The Sn–Cu polymetallic deposit provides an excellent case for understanding the evolution and metallogeny of multi-stage hydrothermal fluids.

In this paper, we examine the evolution of hydrothermal fluid solutions during the life of the hydrothermal system to reconstruct the hydrothermal ore-forming process using fluid inclusions from altered minerals at different ore forming stages. These data are used to discuss variations in ore-forming fluid compositions with decreasing pressure and temperature over time. Finally, a model of ore formation is established using calculations of thermodynamic parameters, including salinity, density, temperature, pressure, and depth of the fluid inclusions.

## GEOLOGICAL BACKGROUND

The giant Gejiu Sn–Cu polymetallic deposit is located along the western margin of the Cathaysia Block, which is a joint region of three blocks consisting of the Yangtze, Indochina, and the Cathaysian (Figure 1). The outcropping strata in the Gejiu area include the Triassic sedimentary formation that consists of carbonate in the lower part, and clastic and carbonate rocks with intercalated basic lavas in the upper part. The most significant fault, the NS-trending Gejiu fault, divides the Gejiu mineralization area into the eastern and the western districts (Figure 1). Other secondary faults cover NE-trending, NW-trending, and the EW-trending faults. The intrusions in the Gejiu district mainly include 1) porphyritic granite and equigranular granite; 2) alkaline rocks; and 3) gabbro–monzonite. These intrusions are exposed in the western part but buried deep in the eastern district (Figure 1). The intrusions buried deep in the eastern district characterized by S-granites with high Sn (12–28 ppm), W (7–28 ppm), F (1,448–2,095 ppm) and B (12–23 ppm) have undergone a high degree of fractionation (Chen et al., 2020). The intrusions exposed in the western district are characterized by I-granites. The Sn–Cu polymetallic deposits are associated with S-granites in eastern Gejiu, and the U–Th–Nb–Ta–REE

mineralizations are related to I-granites in western Gejiu (Chen et al., 2020).

Complex magma differentiation crystallization and post-magmatic hydrothermal evolution may have resulted in a diversity of types of mineralization (Zhang et al., 2008; Chen et al., 2020).

## STYLES OF MINERALIZATION

Three types of ore styles such as skarn, stratabound, and vein type have been recognized in the Gejiu Sn–Cu polymetallic ore district (Figure 2) (308 Geological party, 1984; Mlnlu and Kwak, 1994; Cheng et al., 2012, 2013, 2015).

### Skarn Ore

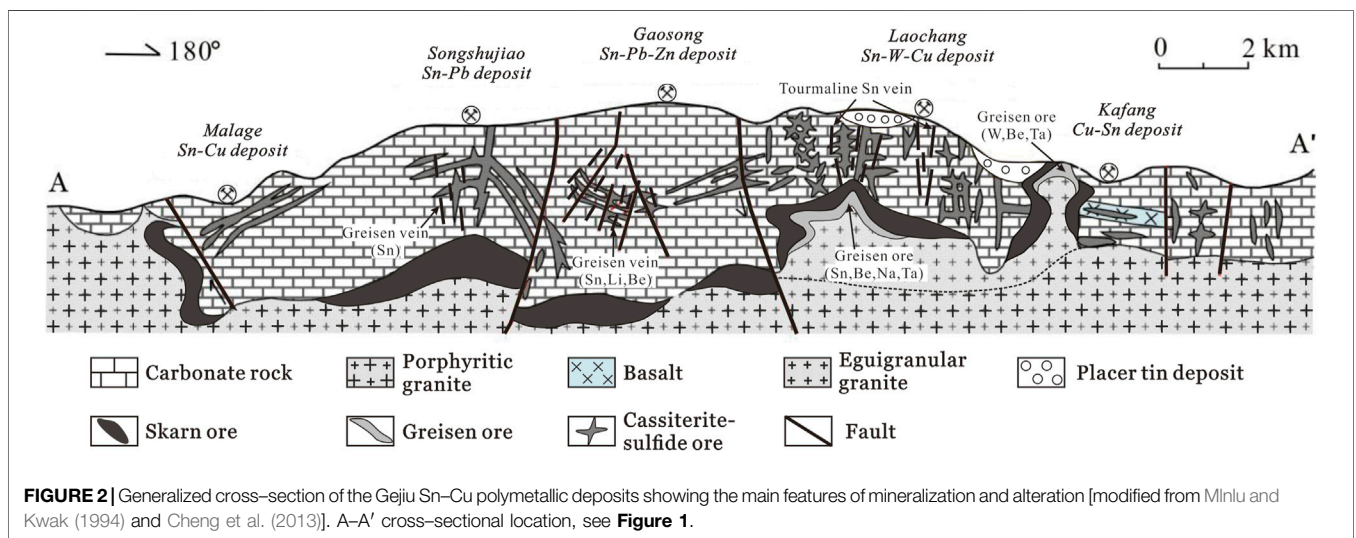
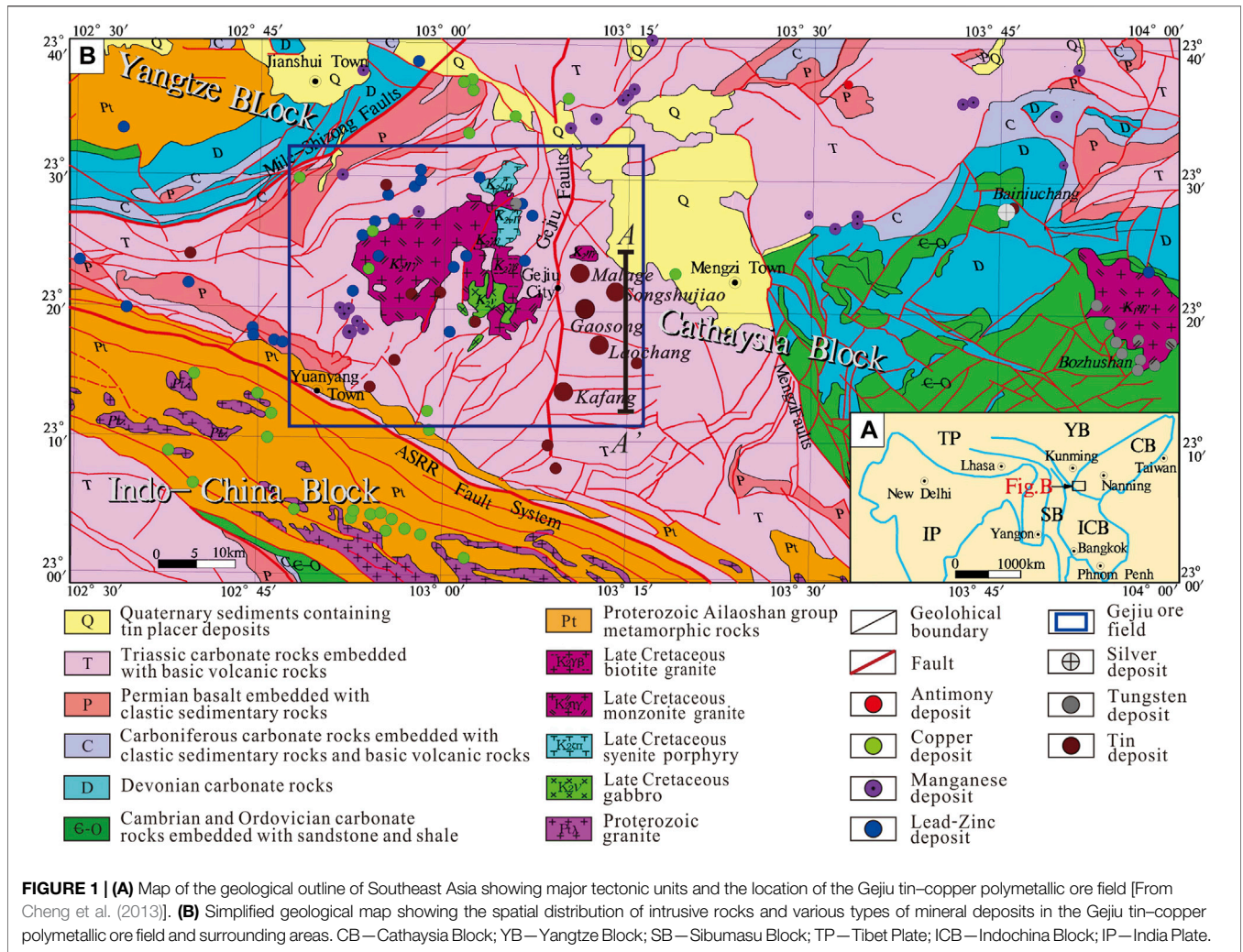
Skarn ore is usually found in the contact zone between granitic intrusions and carbonate wallrocks, and accounts for about 80% of the copper and 30% of tin resources of the Sn–Cu polymetallic deposit (Mlnlu and Kwak, 1994). This style of ore developed in the five large ore deposits shown in Figure 2.

The Malage Sn–Cu deposit has a large ore for Sn and a medium for Cu (Peng, 1985). About 0.14 Mt of tin ore is recoverable at present, with an average grade of 1.16% Sn. The ore minerals include cassiterite, chalcopyrite, sphalerite, galena, molybdenite, magnetite, arsenopyrite, pyrrhotite, and pyrite. Gangue minerals include garnet, diopside, and actinolite. They commonly occur as veins and disseminations in skarn ores. The orebodies are usually sack like, lens shaped, and lenticular (Figure 2). Mineralizations are characterized by a clear metal zonation centered as the Beipaotai porphyritic granite outward: Sn→Cu→Sn→Sn–Cu→Sn–Pb→Pb–Zn–Sn (308 Geological Party, 1984).

The Songshujiao Sn–Pb deposit has a large ore for Sn and a medium for Pb. At present, it contains 1.70 Mt of recoverable tin ore with an average grade of 0.52% Sn, and 1.62 Mt of copper ore with an average grade of 0.46% Cu. The orebodies occur as lenticular, lens shaped, and stratiforms (Figure 2). The ore minerals are cassiterite, chalcopyrite, scheelite, molybdenite, pyrrhotite, arsenopyrite, and pyrite. Gangue minerals include garnet, diopside, and scapolite.

The Gaosong Sn–Pb–Zn deposit is characterized by cassiterite–sulfide ores within the proximal skarn in the contact zone between the Gejiu formation carbonate and Gaosong porphyritic granite (Figure 2). It contains 32.84 Mt of recoverable tin ore with an average grade of 1.02% Sn, and 27.22 Mt of copper ore with an average grade of 0.87% Cu. The sulfide minerals are related to retrograde skarn minerals, including actinolite, tremolite, and chlorite. The major ore minerals cover cassiterite, chalcopyrite, scheelite, molybdenite, arsenopyrite, pyrrhotite, pyrite, and magnetite.

The Laochang Sn–W–Cu deposit has a super-large for Sn, a large for copper, and a medium for Pb and W (Peng, 1985) (Figure 2). It contains 39.76 Mt of recoverable tin ore with an average grade of 0.52% Sn, and 42.86 Mt of copper ore with an average grade of 1.22% Cu. Skarn ores cover Sn, Cu, and W ores. The ore minerals are mainly chalcopyrite, cassiterite, scheelite, pyrrhotite, arsenopyrite, and pyrite. The gangue minerals are mainly garnet, diopside, fluorite, tourmaline, phlogopite, chlorite, and quartz.



The Kafang Cu–Sn deposit has defined reserves of about 40 Mt Cu with an average grade of 1% Cu and >10 Mt Sn with an average grade of 0.7% Sn (Cheng et al., 2012). It contains 10.33 Mt of recoverable tin ore with an average grade of 0.57% Sn, and 20.36 Mt of copper ore with an average grade of 1.2% Cu. The ore minerals include chalcopyrite, cassiterite, scheelite, native gold, sphalerite, galena, molybdenite, pyrrhotite, pyrite, and arsenopyrite. The gangue minerals are mainly garnet, diopside, epidote, actinolite, tremolite, sericite, chlorite, quartz, and calcite.

## Stratabound Ore

In the Malage Sn–Cu polymetallic deposit, stratabound ore with an average grade of 2.39% Sn occurs in some sedimentary rocks far from the granitic intrusions (308 Geological Party, 1984). This stratabound ore also contains a certain amount of Cu, Pb, Zn, In, and Bi in addition to Sn. The alteration minerals cover anhydrous skarn minerals like garnet, pyroxene, diopside, tremolite, and wollastonite, formed in the early skarn stage, and hydrous skarn minerals like epidote and phlogopite, actinolite, chlorite and sericite, developed at a later stage.

In the Songshujiao Sn–Pb deposit, the ores occur mainly in carbonates far from the granitic intrusion. The spatial distribution of the orebodies is controlled by both faults and small folds caused by the granite mound bulge (Figure 2). The major ore minerals are cassiterite, cerussite, malachite, pyrite, and arsenopyrite, and gangue minerals include calcite, quartz, and minor fluorite.

In the Gaosong Sn–Pb–Zn polymetallic ore deposit stratiform like cassiterite–sulfide ores occur mainly in carbonates far from the granitic intrusion that is controlled by strike–slip faults (Figure 2). The cassiterites occur as disseminated grains in the ore with an average Sn grade of about 2% (Guo et al., 2018).

The Laochang ores as reticular veins are hosted in the carbonate rocks. The ore minerals include cassiterite, chalcopyrite, arsenopyrite, and pyrite, and the gangue tourmaline, quartz, and phlogopite. The ore distributions are controlled by granitic intrusions, faults, and host rocks. The granite bodies usually occur about 200–1,000 m beneath the surface (Figure 2).

In the Kafang ore deposit, the stratabound copper–tin ores in tabular form and stratiform occur in the contact metasomatic zone between the granitic intrusion and the Triassic basalt (Figure 2). The ore minerals include chalcopyrite, cassiterite, molybdenite, arsenopyrite, pyrite, and pyrrhotite, and the gangue minerals cover actinolite, tremolite, phlogopite, and fluorite (Cheng et al., 2012).

## Vein-Type Ore

Vein-type ores consisted mainly of tourmaline–cassiterite–quartz veins occurring within carbonate rocks in the Laochang district. The distribution of the ore bodies was controlled by three factors: granitic intrusions, host rocks, and faults (Figure 2). Granitic intrusions occurred 200–1,000 m beneath the surface (Peng, 1985). Tin ores with average grades of 0.42% Sn, 0.11% WO<sub>3</sub>, and 0.13% Be have been found (Cheng et al., 2013).

## Ore-Forming Stages

The mineralization processes can be divided into the following four stages according to ore fabric, mineralogical assemblage and cross-cutting relationships combined with the results of previous

studies (Minlu and Kwak, 1994; Zhuang et al., 1996; Zhang et al., 2012; Liao et al., 2014). The alteration and ore minerals formed at former stage were universally overlapped by later minerals.

Stage I (skarnization): The Gejiu Sn–Cu polymetallic deposits are characterized by contact metasomatic skarn ore between the granite and the wallrocks (Figure 2). High-temperature hydrothermal fluid moved to the contact zone to form anhydrous skarn minerals characterized by garnets (grossular, and almandine) (Figure 3). This mineral assemblage was replaced by subsequent hydrous skarn minerals like actinolite, epidote, and chlorite as well as ore minerals, such as chalcopyrite, bornite, cassiterite, pyrrhotite, and pyrite (Figure 3). The later stage was the main forum for the formation of cassiterite and chalcopyrite. Orebodies of this type are characterized by high Cu (2–5%) and low Sn (0.5–0.8%) contents (Minlu and Kwak, 1994).

Stage II (greisenization): The greisen ore was formed between the skarn ore and the cupola of the granitic intrusion by the alkali metasomatism of the post-magmatic hydrothermal fluid (Figure 2). The granitic magma saturates in volatiles during crysallization and these volatiles play the role of mineralizing fluids, all of the ore-forming components originate from the magma with activity of fluorine and boron, and eventually led to the formation of Sn–W–B–Nb–Ta ore veins (Figure 2). The greisen ore veins were characterized by such mineral assemblages as cassiterite, wolframite, fluorite, tourmaline, mica, and quartz (Figure 3). Orebodies of this type are characterized by high Sn (2–3%) and low Cu (<0.5%) (Minlu and Kwak, 1994).

Stage III (cassiterite–sulfide): Large amounts of cassiterite, chalcopyrite, pyrite, galena, and pyrrhotite were formed in this stage. The cassiterites were light-brown fine-grained crystals together with chalcopyrite and fluorite (Figure 3). The chalcopyrites were intergrown with galena, pyrite, and other minerals (Figure 3). The cassiterite–sulfide veins of this stage cut the early-stage ores (Figure 3), and the chalcopyrites occurred in gaps among garnets and replaced garnets along the edge of garnets (Figure 3). This implies that this mineral assemblage was formed after stage II. The cassiterites in the mineral assemblage were encompassed by sulfide minerals, implying that they had been formed earlier than the sulfide minerals (Figure 3). These ore minerals took up approximately 30% of the total tin resources in the Laochang ore deposit (Minlu and Kwak, 1994).

Stage IV (cassiterite–tourmaline–quartz): This was the last stage in the ore-forming process. The ore minerals include cassiterite, galena, sphalerite, and pyrite, and the gangue minerals cover mainly of needle-like tourmaline and quartz occurring in stockwork veins (Figure 3). They usually occur in the upper part of individual deposits and cut stratabound ore bodies (Figure 2). The ores occur in weak tin mineralizations with an approximately average grade of Sn of 0.1%.

## FLUID INCLUSION

### Sampling and Methods

Samples from stage I (chalcopyrite–bornite–pyrrhotite, Figure 3), stage II (cassiterite–bearing greisen ore, Figure 3), stage III

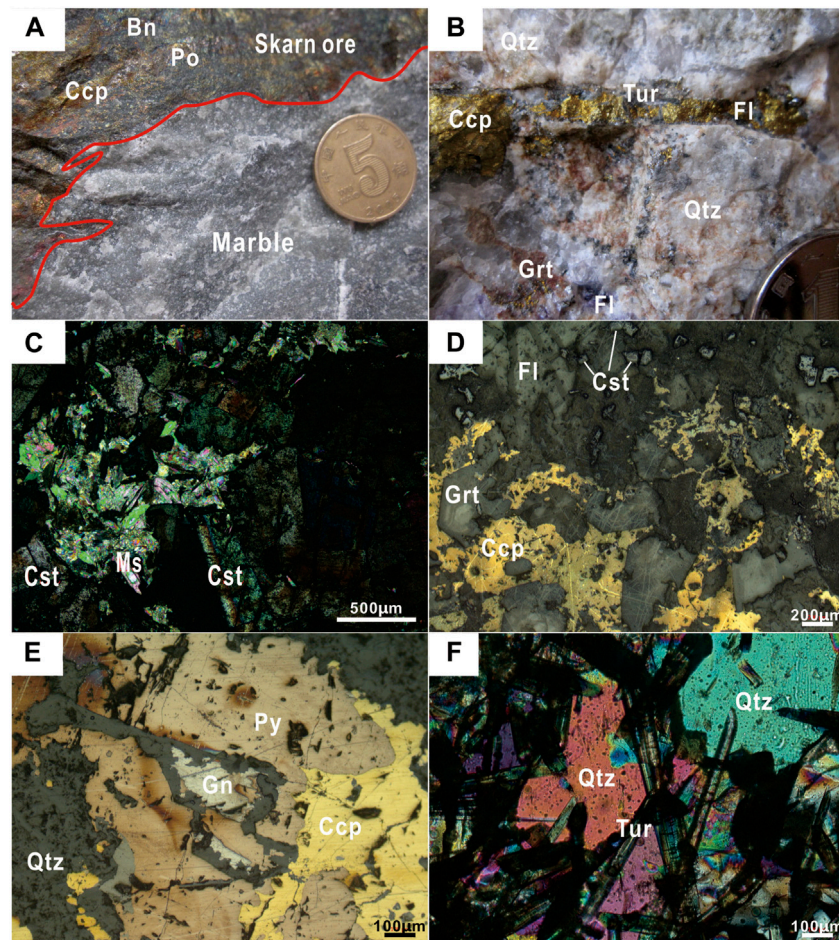


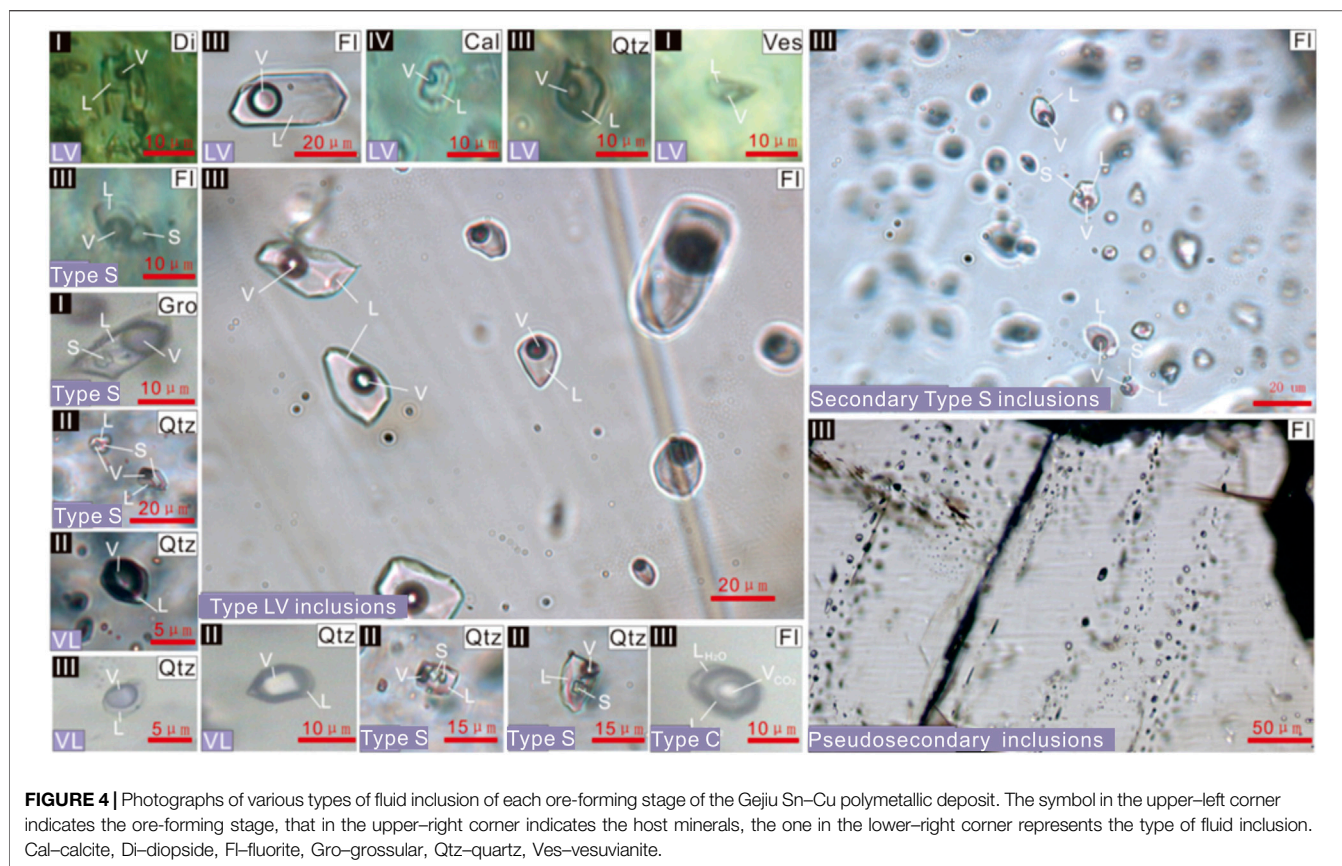
**FIGURE 3** | Hand specimens and microscopic photos showing the field characteristics, alteration mineral associations, and their intergrowth-related relationships from the Gejiu Sn-Cu polymetallic ore deposit: Bn-bornite, Ccp-chalcopyrites, Cst-cassiterites, Fl-fluorite, Gn-galena, Grt-garnet, Ms-mica, Po-pyrrhotite, Py-pyrite, Qtz-quartz, Tur-tourmaline.

(cassiterite-chalcopyrite-fluorite, **Figure 3**, chalcopyrite-galena-pyrite-quartz, **Figure 3**, chalcopyrite-fluorite-tourmaline vein, **Figure 3**), and stage IV (cassiterite-tourmaline-quartz veins, **Figure 3**) were collected from levels 1,598 and 1,990 of mining tunnel 18-1 from the orebody of the Dadoushan ore block in the Laochang ore deposit, the 8006 branch mining tunnel of the Tangziao ore block, and samples from the Songshujiao and Kafang ore deposits. Both sides of each sample were polished so that they were 0.2–0.3 mm thick. Following this, 34 samples from the four ore-forming stages were selected to use for the fluid inclusion study by utilizing optical petrography, microthermometry, and Raman spectroscopy (**Supplementary Table 1**). The microthermometry of fluid inclusions was conducted with a Linkam MDS 600 heating-freezing stage at the State Key Laboratory of Geological Processes and Mineral Resources (GPMR) at the China University of Geosciences in Wuhan. The precision of the temperature measurements was approximately  $\pm 0.1$  and  $\pm 2^\circ\text{C}$  for freezing and heating, respectively. The heating/freezing rates generally varied from 0.2 to  $5^\circ\text{C}/\text{min}$ , but decreased to less than  $0.2^\circ\text{C}/\text{min}$  near the

phase transformation. The laser Raman spectroscopic data were also obtained at the GPMR by using a Renishaw RW-1000 Raman microspectrometer. An argon ion laser with a wavelength of 514.5 nm was used for detection at  $25^\circ\text{C}$ . The spectral range was between  $1,000$  and  $4,000\text{ cm}^{-1}$  when analyzing  $\text{CO}_2$ ,  $\text{N}_2$ , and  $\text{CH}_4$ . A total of 677 valid data items from the various fluid inclusions were thus obtained.

**Salinity calculation:** For the  $\text{NaCl-H}_2\text{O}$  system, in case of low-salinity fluid inclusions,  $\omega(\text{NaCl}_{\text{eq}}) < 26.3\%$ , that do not contain daughter minerals or high-salinity fluid inclusions,  $\omega(\text{NaCl}) > 26.3\%$ , that do contain daughter minerals, the salinity of the inclusions is calculated according to the formula proposed by Bakker (1999 and 2018). For the  $\text{H}_2\text{O-NaCl-CO}_2$  system, the salinity of the inclusions is calculated according to the formula proposed by Bakker (1999, 2018).

**Density calculation:** For  $\text{NaCl-H}_2\text{O}$  solution inclusions with different salinities, density is calculated by fitting the density formula based on experimental values provided by Bakker (1999, 2018). For fluid inclusions of unsaturated brine-vapor boiling, in case the salinity is low, the fluid density of gas phase inclusions



coexisting with the liquid phase are approximated using the formula proposed by Bakker (1999, 2018). The density of C-type inclusions is obtained by using a diagram of the relationship between homogeneous temperature and the CO<sub>2</sub> phase density of the inclusions proposed by Shepherd et al. (1985).

**Estimation of pressure and depth:** Fluid inclusions may provide estimation of trapping pressure using the formula proposed by Shao and Mei (1986). But the ore-forming depth cannot be simply estimated because the trapping pressures may be either lithostatic or hydrostatic, or somewhat in between. In this study the depths were approximately calculated based on the estimated fluid pressures using the method proposed by Sibson (2001, 2004) with reference to the research works by Rusk et al. (2008) and Fournier (1999).

## Petrography and Classification

Liquid-rich aqueous (type LV), vapor-rich aqueous (type VL), and solid-bearing (type S), and aqueous-carbonic (type C) inclusions are recognized based on their number, nature, and proportion of phases (liquid-vapor-solid) at room temperature (Bakker, 1999; Bakker, 2018). These inclusions are from grossular, diopside, fluorite, vesuvianite, quartz, and calcite occurring in different stages of ore formation, and are used to record the progressive pressure, temperature, and compositional evolution of the hydrothermal ore-forming fluids of the Gejiu ore deposits.

The Gejiu ore deposits are rich in fluid inclusions. Liquid-rich aqueous (type LV), vapor-rich aqueous (type VL), aqueous-carbonic (type C), and solid-bearing (type S) inclusions are distinguished in terms of their number, nature, and proportion of phases (liquid-vapor-solid) at room temperature (Bakker, 1999; Bakker, 2018).

Type-VL inclusions contain liquid and vapor phases with a 50–90 vol% vapor at room temperature. When being heated to homogenization, the inclusions with a gas phase are commonly observed in minerals of skarn and greisen, and have sizes ranging from 8 to 60 μm. Their shapes are irregular and oblate, and they are dark in color. These inclusions illustrate uneven distribution, and coexist with other types of inclusions (**Figure 4**).

Type-LV inclusions contain liquid and vapor phases at 5–50 vol% vapor at room temperature. When being heated to homogenization, the inclusions form a single liquid phase. Such inclusions commonly occur in all stages of mineralization, and exhibit sizes varying from 3 to 86 μm. They have irregular, elongated, oblate, and negative crystal shapes. In fluorite and quartz, these inclusions commonly occur along a growth zone (**Figure 4**), implying that they have a primary origin.

Type-S inclusions contain three phases (liquid + vapor + solid), and account for 15–25% of all inclusions. According to method of heating, they can be subdivided into two categories. The first consists of unsaturated daughter crystal inclusions (type

**TABLE 1** | Summary of fluid inclusion data for each stage of the of the Gejiu Sn-Cu polymetallic deposits.

| Ore-forming stage                          | Ore deposit | Number | $T_{m,ice}$ (°C)  | Th (°C) (mean)   | Salinity wt% NaCl <sup>a</sup> | Density <sup>a</sup> (g/cm <sup>3</sup> ) | Pressure (MPa) <sup>b</sup> | Depth (Km) <sup>c</sup> |
|--|-------------|--------|-------------------|------------------|--------------------------------|---|-----------------------------|-------------------------|
|  |             |        |                   |                  |                                |   | Range                       | Range                   |
| Stage I: Skarnization                      | Kafang      | 55     | -1.8<br>to -14.2  | 353-582<br>(485) | 3.06-67.07                     | 0.160-1.267                               | 118-150                     | 7.0-8.23                |
|  | Laochang    | 39     | -3.7<br>to -11.3  | 345-503(408)     | 6.01-15.27                     | 0.429-0.783                               | 108-138                     | 6.63-7.82               |
|  | Songshujiao | 31     | -5.5<br>to -7.6   | 332-600<br>(493) | 8.55-11.22                     | 0.192-0.550                               | 126-156                     | 7.36-8.43               |
|  | Sum         | 125    | -1.8<br>to -14.2  | 343-562<br>(464) | 5.87-31.29<br>(15.30)          | 0.260-0.87(0.57)                          | 117-148(133)                | 7.0-8.20(7.6)           |
| Stage II: Greisenization                   | Tangziao    | 34     | -6.8<br>to -16.9  | 317-597<br>(392) | 10.24-52.7                     | 0.685-1.287                               | 102-131                     | 5.71-8.86               |
|  | Laochang    | 11     | -10.7<br>to -16.0 | 284-549<br>(361) | 14.67-19.4                     | 0.470-0.901                               | 83-153                      | 5.46-8.35               |
|  | Songshujiao | 32     | -2.0<br>to -9.4   | 252-461<br>(348) | 3.39-13.29                     | 0.504-0.837                               | 67-126                      | 4.57-7.36               |
|  | Sum         | 79     | -2.0<br>to -16.0  | 284-536<br>(367) | 9.43-28.46<br>(18.59)          | 0.553-1.01(0.782)                         | 84-136(110)                 | 5.50-7.75(6.63)         |
| Stage III: Cassiterite-sulfide             | Kafang      | 17     | -2.3<br>to -11    | 195-280          | 3.87-15.07                     | 0.815-0.937                               | 54-77                       | 3.88-5.14               |
|  | Tangziao    | 65     | -1.1<br>to -18.9  | 102-482          | 1.91-39.76                     | 0.378-1.091                               | 85-116                      | 2.8-7.0                 |
|  | Laochang    | 128    | -2.5<br>to -20.8  | 120-431          | 4.18-22.91                     | 0.547-1.017                               | 37-125                      | 2.7-7.0                 |
|  | Songshujiao | 135    | -0.1<br>to -20.7  | 126-432          | 0.17-22.85                     | 0.534-1.03                                | 48-87                       | 2.20-6.20               |
|  | Sum         | 426    | -2.5<br>to 20.7   | 136-482<br>(256) | 2.53-25.15<br>(11.65)          | 0.568-1.02(0.794)                         | 56-101(78.5)                | 4.0-6.24 (5.12)         |
| Stage IV:<br>Cassiterite-tourmaline-quartz | Kafang      | 15     | -4.2<br>to -4.6   | 133-184          | 6.74-7.31                      | 0.936-0.982                               | 36-50                       | 3.60-5.0                |
|  | Songshujiao | 21     | -0.1<br>to -0.4   | 139-250          | 0.18-0.70                      | 0.671-0.892                               | 23-40                       | 2.30-4.00               |
|  | Sum         | 36     | -0.1<br>to -4.6   | 136-217<br>(182) | 3.46-4.01<br>(3.27)            | 0.804-0.937<br>(0.871)                    | 30-45 (36)                  | 3.0-4.5 (2.75)          |

<sup>a</sup>Salinities and density calculated using method proposed by Bakker (1999, 2018).

<sup>b</sup>Pressures calculated using method proposed by Shao and Mei (1986).

<sup>c</sup>Depths estimated using method proposed by Sibson (2001, 2004).

$T_{m,ice}$ -final melting temperature of ice; Th-homogenization temperature. H-Ore-forming depth.

US). During heating, the daughter crystals disappear first, followed by the disappearance of the bubbles to uniform a liquid phase consisting of unsaturated fluids. Their sizes vary from 12 to 20  $\mu\text{m}$ , and they has a gas-liquid ratio of 15-25%. The second category consists of supersaturated inclusions containing daughter crystals (type OS). During heating, the bubbles disappear, followed by the daughter crystals, into a homogeneous liquid phase to form a supersaturated fluid. Their sizes vary from 6 to 12  $\mu\text{m}$ , and the ratio of gas to liquid is approximately 10-25% by volume. These inclusions are observed only in cassiterite-sulfide (stage III) minerals, The morphology of some daughter minerals is more regular, and they are determined to be halites (Figure 4). Diamond daughter minerals (Figure 4) were also observed, and are brucite or calcite according to their shapes.

Type-C inclusions consists of vapor  $\text{CO}_2$ , liquid  $\text{CO}_2$ , and brine solutions (S-type) that developed only in quartz-fluorite veins formed in stage III (Figure 4). They account for approximately 10-30% of all inclusions. The  $\text{CO}_2$  in the gas and liquid phases is first homogenized to a uniform liquid phase with the brine solution during the heating process. These

inclusions vary in size from 8 to 20  $\mu\text{m}$ , and display mostly elliptic and polygonal shapes (Figure 4). The volume of the  $\text{CO}_2$  liquid phase is 40-70%, and that of  $\text{CO}_2$  gas is 10-20%.

## Microthermometry

A summary of microthermometric data for fluid inclusions in this study is illustrated in Table 1. The graphical results of microthermometry are shown in Figures 5-7.

Stage I (skarnization): Types-LV, -VL,-OS, and-US inclusions were all developed. Types-LV and-VL inclusions account for 60 and 40%, respectively, of all inclusions (Figure 4). The host minerals of the inclusions are garnet, diopside, and vesuvianite. The most homogeneous temperature of the fluid inclusions range from 332 to 560°C with an average of 464°C (Table 1; Figure 5A). The final melting temperatures of ice of type-(LV + VL) inclusions range from -1.8 to -14.2°C, with corresponding salinities of 3.06 wt% NaCl to 66.75 wt% NaCl (Table 1; Figure 5B). The densities calculated using the formula proposed by Bakker 1999; Bakker 2018 range from 0.160 to 1.267 g/cm<sup>3</sup> (Table 1), and most of them vary from 0.5 to 0.80 g/cm<sup>3</sup> (Table 1; Figure 7). The trapping pressure from

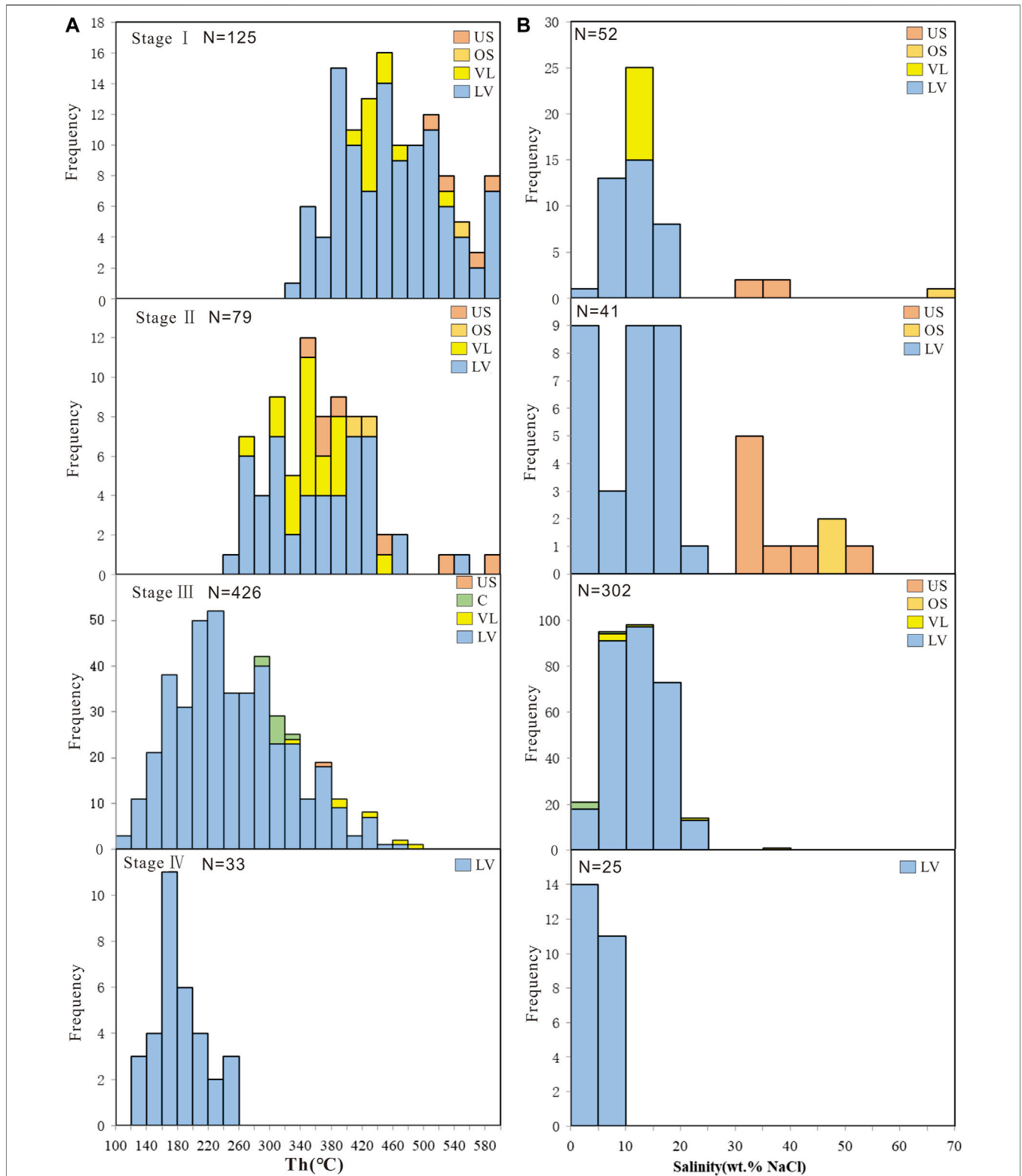
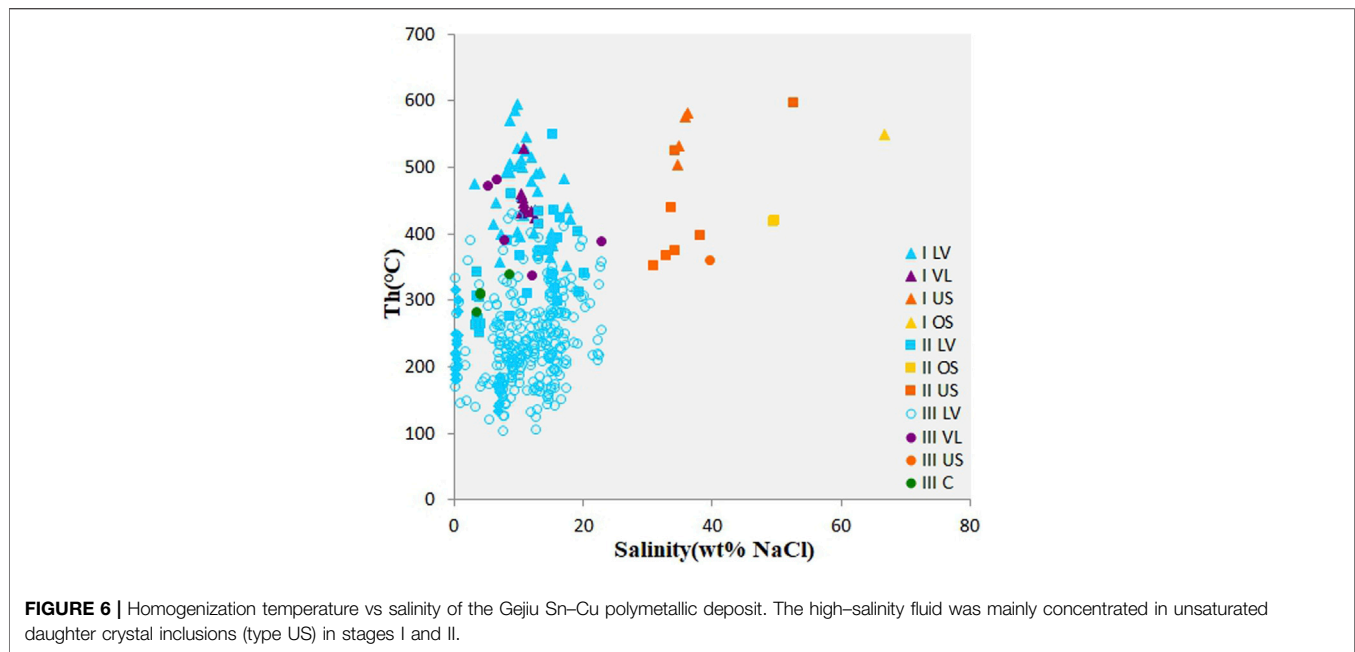


**FIGURE 5 |** Histogram of the relative frequencies of the homogeneous temperature **(A)** and salinity **(B)** of fluid inclusions in each stage of the Gejiu Sn-Cu polymetallic deposit.



these inclusions was estimated to range from 117 to 148 MPa using the formula proposed by Shao and Mei (1986) (Table 1).

Stage II (greisenization): The host mineral of the inclusions measured in this study was quartz. Similar to the skarnization stage, types–LV, –VL, –OS, and–US inclusions fluid inclusions had developed in this stage. The most homogeneous temperature of the fluid inclusions vary from 284 to 536°C with an average of 367°C (Table 1; Figure 5A). The final melting temperatures of ice for type–(LV + VL) inclusions range from –2 to –16°C, with corresponding salinities of 3.39 wt% NaCl to 53.4 wt% NaCl, and a mean of 18.59% wt% (Figure 5B). The densities calculated using the formula proposed by Bakker 1999; Bakker 2018 range from 0.470 to 1.194 g/cm<sup>3</sup>, and are mainly concentrated at 0.64–0.88 g/cm<sup>3</sup> (Table 1; Figure 7). The trapping pressure from these inclusions is estimated to range from 84 to 136 MPa using the formula proposed by Shao and Mei (1986) (Table 1).

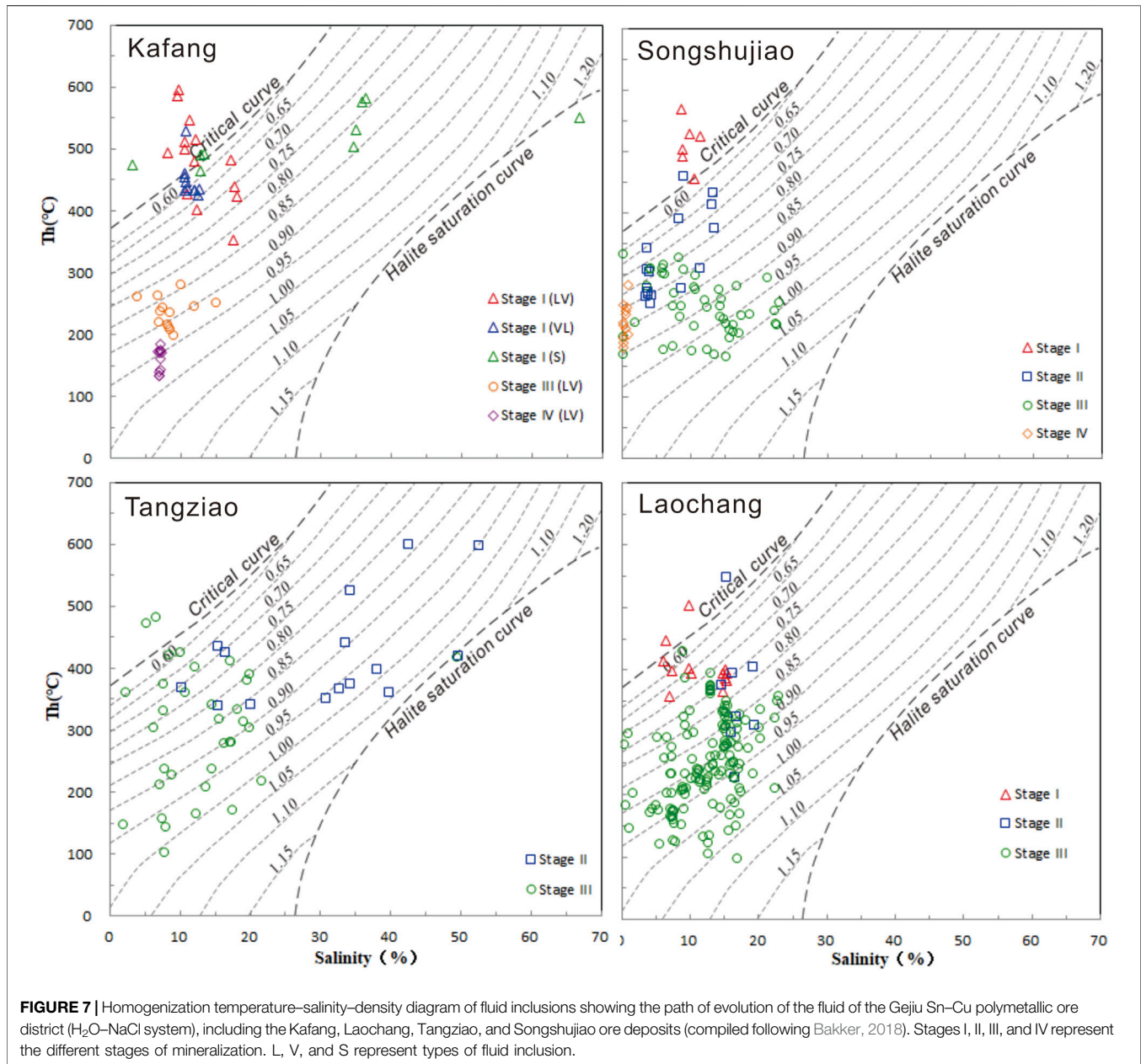
Stage III (cassiterite–sulfide): The host minerals of inclusions measured in this study include fluorite and quartz. LV, VL, C, and US fluid inclusions had developed in this stage. The homogeneous temperature of fluid inclusions vary from 136 to 482°C, and most of it range from 180 to 320°C with a mean of 256°C (Table 1; Figure 5A). The final melting temperature of ice for type–(LV + VL) inclusions rang from –2.5 to –20.7°C, with corresponding salinities of 0.17 wt% NaCl to 39.76 wt% NaCl and a mean of 11.65 wt% NaCl (Table 1; Figure 5B). The densities calculated using the formula proposed by Bakker 1999; Bakker 2018 range from 0.378 to 1.091 g/cm<sup>3</sup>, and are mainly concentrated at 0.65–1.05 g/cm<sup>3</sup> (Table 1; Figure 7). There is a large difference between high and low salinities, which is inferred to result from the mixing of different solutions acting as source fluid. The trapping pressure from these inclusions is

estimated to range from 56 to 101 MPa using the formula proposed by by Shao and Mei (1986) (Table 1).

Stage IV (cassiterite–tourmaline–quartz): The host mineral of inclusions measured in this study is calcite. In this stage, only type–LV inclusions are identified in calcite. The microthermometric homogenized temperatures range from 136 to 217°C with a mean of 182°C, and are mainly concentrated in the range 160–180°C (Table 1; Figure 5A). The final melting temperatures of ice for the type–(LV) inclusions range from –0.1°C to –4.6°C, with corresponding salinities of 0.18 wt% NaCl to 7.31 wt% NaCl, and a mean of 3.27% wt% NaCl [Table 1; Figure 5B]. The densities calculated using the formula proposed by Bakker 1999; Bakker 2018 range from 0.671 to 0.982 g/cm<sup>3</sup>, and are mainly concentrated at 0.80–0.97 g/cm<sup>3</sup> (Table 1; Figure 7). The trapping pressure from these inclusions was estimated to range from 30 to 45 MPa using the formula proposed by Shao and Mei (1986) (Table 1).

## Composition of Fluid Inclusions

The results of laser Raman spectroscopy show that CH<sub>4</sub> and CO<sub>2</sub> are detected in fluid inclusions captured in the host minerals in all deposits in addition to the Kafang ore deposit, and N<sub>2</sub> is detected in inclusions from some ore bodies of the Laochang deposit (Figure 8). The liquid composition of the inclusions is mainly H<sub>2</sub>O, and they contain a small amount of liquid CO<sub>2</sub>. The CH<sub>4</sub> content of the inclusions had decreased whereas the CO<sub>2</sub> content had increased slightly from stage I to stage IV. The daughter minerals include halite, calcite (Figure 8J), and sylvite. S-type inclusions are observed only in stage III (Figure 4). Thus, the fluids in stages I and II from the H<sub>2</sub>O–NaCl system, and those from stage III belong to the H<sub>2</sub>O–NaCl–CO<sub>2</sub> system (Liao et al., 2014).



## Depth of Mineralization

The emplacement depth of granitic intrusions is an important factor in controlling mineralization processes, especially for controlling the granite-related mineralization. Magmatic–hydrothermal processes can result in tin and copper mineralization at both shallow and deep levels of emplacement, and the relative importance of these processes changes as a function of pressure (Linnen, 1998). Prokofev and Pek (2015) illustrated that As the ore-forming depth decreases there was a conjugate regressive trend in the evolution of temperature and pressure of ore-forming fluids from  $P_{\text{max}}$  (maximum pressure value) and  $T_{\text{max}}$  (maximum temperature value) to  $P_{\text{min}}$  (minimum pressure value) and  $T_{\text{min}}$  (minimum temperature value) under physical restrictions

of maximum and minimum fluid pressure by lithostatic and hydrostatic pressure, respectively, and minimum temperature corresponding to geothermal background temperature at the mineral deposition depth. A good correlation between them indicates that estimations of the hydrothermal deposits formation depth using thermobar–geochemical data is justified, and deserves further exploration.

Fluid pressures in a fracture zone show vertical zonation. That is, with the depth change, the fluid pressure in fracture zone regularly changes (Sibson, 2001; Sibson, 2004). According to  $\lambda_V$  (ratio of fluid pressure to lithostatic pressure) the fracture zone with fluids can be divided into three regimes: 1) hydrostatic regime ( $\lambda_V < 0.4$ , depth  $< 5$  km); 2) suprahydrostatic regime ( $0.4 < \lambda_V < 1.0$ , depth = 5–16 km); 3) lithostatic regime ( $\lambda_V > 1.0$ ,

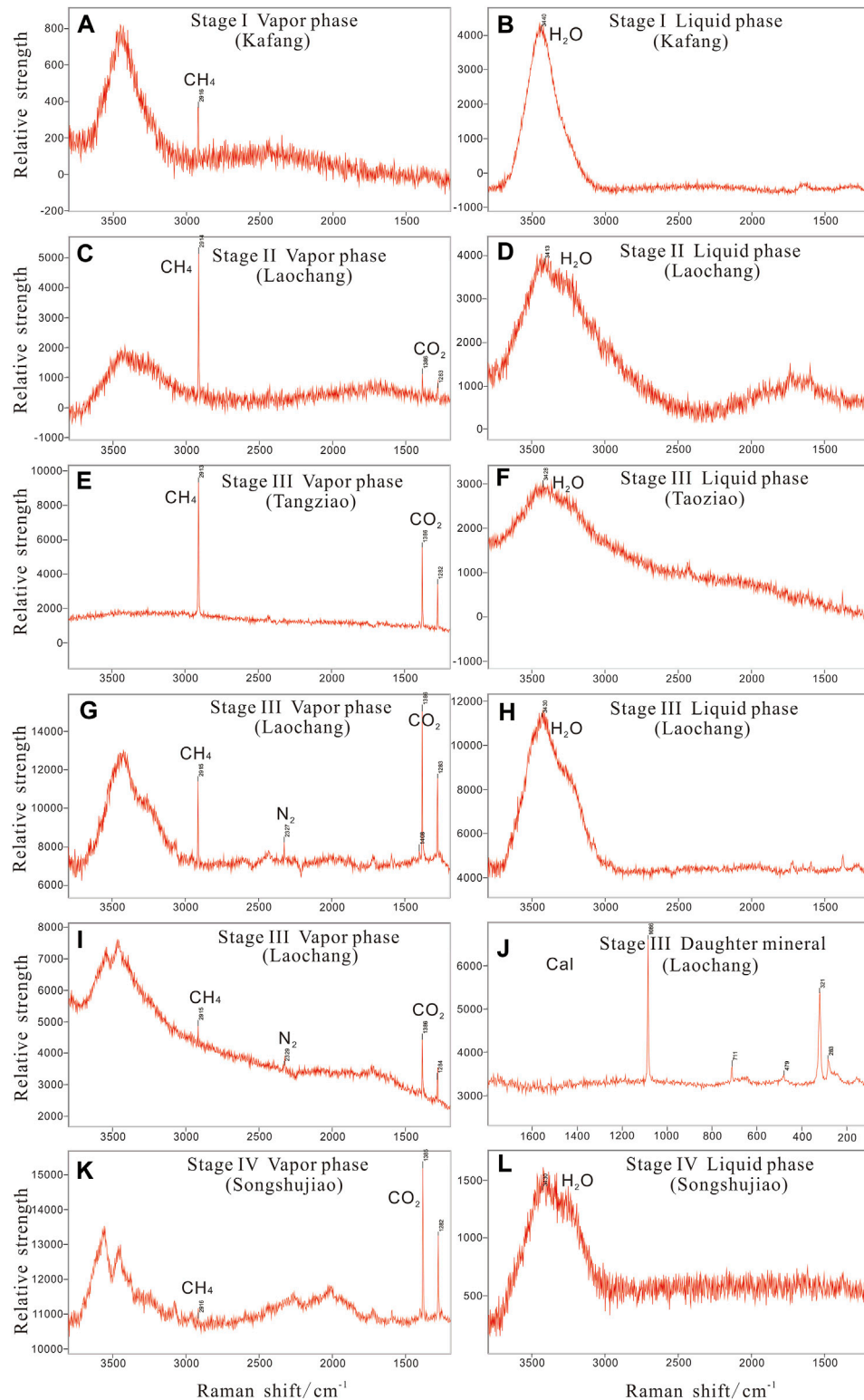


**FIGURE 8** | Representative Raman spectra of fluid inclusions in the Gejiu Sn-Cu polymetallic deposits. **(A)** Type-VL inclusion in stage I from Kafang. **(B)** Type-LV inclusion in stage I from Kafang. **(C)** Type-VL inclusion in stage II from Laochang. **(D)** Type-LV inclusion in stage II from Laochang. **(E)** Type-VL inclusion in stage III from Tangziao. **(F)** Type-LV inclusion in stage III from Tangziao. **(G)** Type-VL inclusion in stage III from Laochang. **(H)** Type-LV inclusion in stage III from Laochang. **(I)** Type-VL inclusion in stage III from Laochang. **(J)** Type-US inclusion in stage III from Laochang. **(K)** Type-VL inclusion in stage IV from Songshujiao. **(L)** Type-LV inclusion in stage IV from Songshujiao.

depth >16 km). Within the hydrostatic regime, the depth is less than 5 km (or fluid pressure is less than 40 MPa), a hydrostatic pressure gradient can be used to estimate the ore-forming depth. Within the hydrostatic regime (the depth is greater than 16 km), the fluid pressure is close to the lithostatic pressure, and the ore-forming depth can be estimated approximately by the lithostatic pressure gradient. However, within 5–16 km (or pressure at 40–370 MPa), there is a nonlinear relationship between the fluid pressure and depth, and the actual pressure of the fracture zone fluid varies from shallow to deep between the lithostatic pressure and the hydrostatic pressure. The formation depths of the Gejiu ore deposits at different ore-forming stages estimated based on Sibson (2001, 2004) are 7.0–8.2 km for Stage I (skarn), 5.5–7.75 km for Stage II (greisen), 4.0–6.24 km for Stage III (cassiterite-sulfidation), and 3.0–4.5 km for Stage IV (cassiterite-tourmaline-quartz).

It has been illustrated based on the analysis of data on the age-frequency distribution of ore deposits that the exhumation rate of epithermal gold, porphyry copper, and orogenic gold deposits are 167, 167, and 63 m/Ma, respectively (Kesler and Wilkinson, 2006; 2009). The emplacement ages of the Gejiu granitic complex range from 78 to 87 Ma (Chen et al., 2020). The estimated exhumation depths of the Gejiu ore district are of 4.90–5.48 km based on the exhumation rate of orogenic gold deposits, which is approximately consistent with the estimated ore deposits formation depth (at present mining depths of the Gejiu mine district vary from 0.5 to 2 km below the ground surface).

## DISCUSSION

### Evolution of Ore-forming Fluid

The microthermometric data show that the ore-forming fluid evolved from a high temperature with a low-to-high salinity to a low temperature with low salinity (Table 1). This is similar to the evolution of magmatic fluids of the mineralization of porphyry Cu at different depths and temperatures described by Fournier (1999). Most porphyry-type deposits apparently deposit ores at ~1–5 km depth, and there is one exception, the porphyry Cu–Mo deposit in Butte formed at depths between 6 and 9 km (Rusk et al., 2008). In the Gejiu Sn–Cu polymetallic deposit the granitic magma intruded to depths of 7–8 km beneath the sedimentary rocks dominated by carbonates, and caused a large region surrounding the hot intrusive magma to attain temperatures above 600°C, which led the host rocks to behave in a plastic manner. The principal stress was the lithostatic load owing to overlying rocks. Fluids with an average salinity of 5.87–31.29 wt% NaCl (Table 1) and gas exsolved from crystallizing magma accumulated and produced dual metasomatism in the zone of contact between the granitic intrusion and the carbonatic rocks to form skarn with Sn–Cu polymetallic mineralization in stage I at temperatures between 343 and 562°C, and under pressures ranging from 117 to 148 MPa, corresponding to the depths of 7.0–8.2 km (Table 1; Figures 2, 10). Almost at the same time, hypersaline brine fluids with an average salinity of 9.43–28.46 wt % NaCl within the inner zone of the intrusions formed greisen

with Sn–B–Nb–Ta mineralization in stage II at temperatures between 284 and 536°C, and under pressures of 84–136 MPa, corresponding to the depth of 5.50–7.75 km (Table 1; Figures 2, 10). A narrow, self-sealed zone consisting of relatively impermeable plastic material separated the region of lithostatic pressure from that where the meteoric water-derived hydrothermal fluids circulate through brittle rocks away from the hot intrusions at hydrostatic pressure. In particular when magma moved upward in a surge, the hypersaline fluids and gas were expelled quickly from the normally plastic region into the brittle region to meet the meteoric water forming mixing fluids with an average salinity of 2.53–25.15 wt% NaCl, temperatures of 136–482°C, and under fluid pressures of 56–101 MPa, corresponding to the depth of 4.0–6.24 km (Table 1; Figures 2, 10). In this case, epithermal veins with cassiterite-sulfide assemblage were deposited in stage III as a result of the decompression and cooling of the magmatic fluid. The relatively dilute fluid that separated from the boiling fluids as a result of decompression greatly influenced the type of mineralization when the fluid moved upward through cooler and brittle rock. The breaking of the self-sealed zones was healed by mineral deposition, and re-breaking resulted in banded epithermal cassiterite-galena-sphalerite-cerargyrite veins in the Songshujiao deposit in stage IV, the ore-forming fluids with an average salinity of 3.46–4.01 wt% NaCl, temperature varying from 136 to 217°C, and under pressures ranging from 30 to 45 MPa, corresponding to the depth of 3.0–4.5 km (Table 1; Figures 2, 10). Eventually, intrusive activity declined and ended, accompanied by hydrothermal activity owing to hydrostatic pressure dominated by meteoric water.

### Ore-forming Mechanism Fluid Boiling and Immiscibility

In the Gejiu Sn–Cu polymetallic deposit, the main ore-forming elements are tin and copper, and occur as cassiterite and chalcopyrite, respectively. The cassiterites were formed mainly in stage II with an average temperature 367°C and stage III with an average temperature 256°C (Table 1; Figure 5). The chalcopyrites precipitated in stages I with an average temperature 464°C and in stage III with an average temperature 256°C (Table 1; Figure 5). As the fluid evolved to stage III, it started boiling and became immiscible with dramatically decreasing pressure of the fluid system. It has been shown by the fluid inclusion studies that the copper precipitate temperature range is similar to the that of the lithostatic pressure converted to hydrostatic pressure (Fournier, 1999; Figure 9). Dropping drastically in pressure disrupted the physicochemical system balance of the ore-forming fluid (Figure 9), resulting in fluid boiling and immiscibility, volatile substances escape from the fluid system, causing significant change of the pH, Eh of the solution and ore minerals precipitation (Hedenquist et al., 1998; Logan, 2000; Meinert et al., 2005). As temperatures decreased, H<sub>2</sub>O–CO<sub>2</sub> fluid immiscibility occurred, yielding high CO<sub>2</sub> inclusions (Roedder, 1992). Thus a sharp increase in CO<sub>2</sub> concentration at stage III (Figure 8) may provide an evidence for fluid immiscibility. A direct link between copper deposition and

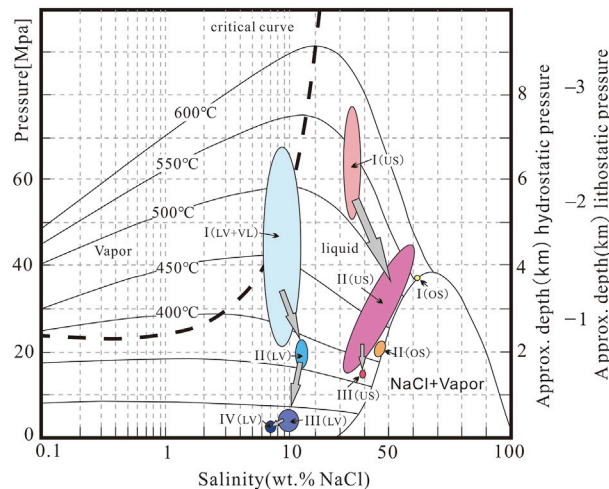


**FIGURE 9** | Phase diagram of ore-forming fluid inclusion showing the path of evolution of the fluid ( $\text{H}_2\text{O}$ - $\text{NaCl}$  system) [drawn following Liao et al. (2014); Bakker (2018)]. In the skarn stage (I), the ore-forming fluid under near the critical state evolved from a low-through-moderate to a high-salinity fluid. In the greisen stage (II), the fluid separated into a coexisting liquid and a vapor phase. The liquid phase had a salinity of 10 wt% NaCl, and that of the coexisting vapor phase was 2 wt% NaCl at 400°C. For the mixing of the meteoric and the magma fluids, the salinity of the type VL inclusions in stage III could not be calculated accurately. A detailed discussion of the evolution of the fluid is provided in the text. Stages I-IV represent the different stages of mineralization. LV, VL, OS, and US are the types of fluid inclusions, see text in detail.

boiling is evident in most veins (**Figure 3**), wherein veins that exhibit boiling and immiscibility have the highest copper grade (Liao et al., 2014). Thus, fluid boiling and immiscibility are probably the most important factor influencing mineralization.

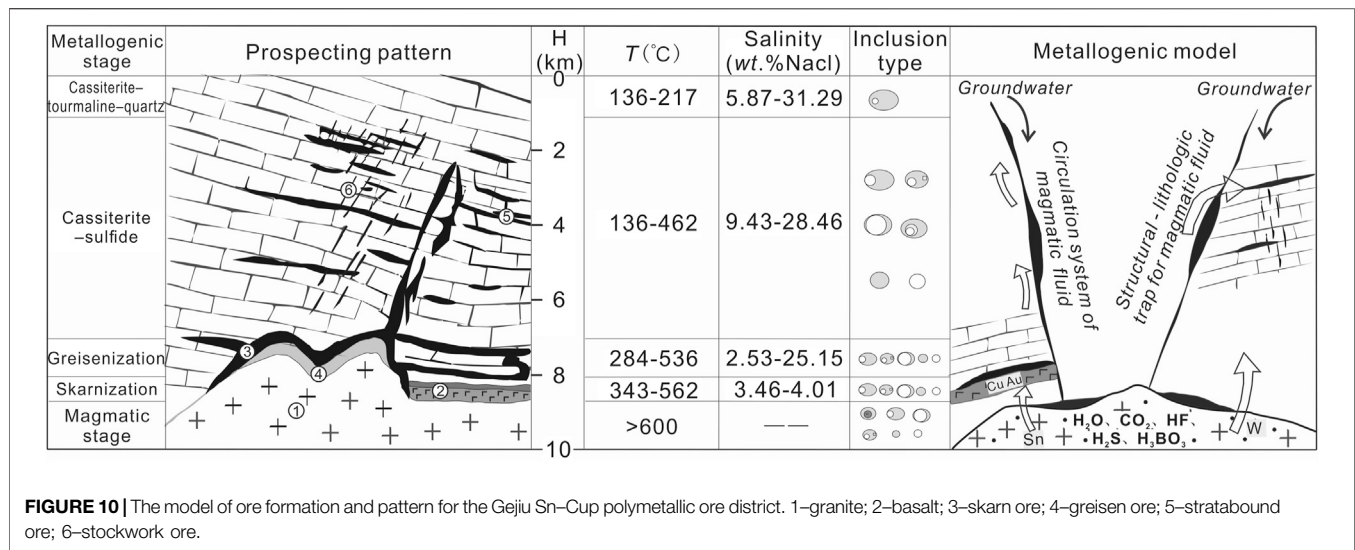
### Mixing of Fluids From Different Sources

In W-Sn hydrothermal ore deposits, another key factor influencing the accumulation ore minerals is the mixing of the fluid (Audíat et al., 2000; Lu et al., 2003; Zhou et al., 2007). The mixing of fluids in the Gejiu Sn-Cu polymetallic deposits took mainly place in stage III. Type C inclusions are much abundant in the fluid at stage III than stage II and  $\text{N}_2$  emerged in stage III (**Figure 8**), which indicate that mixing of external substances to the fluid system (Liao et al., 2014). The addition of  $\text{CO}_2$  could increase the extent of immiscibility greatly (Roedder, 1992). Moreover the concentration effect of losing volatile substances during fluid boiling and immiscibility can result in slightly increased salinity (Henley and McNabb, 1978; Meinert et al., 2003; Wilkinson, 2001). However, the microthermometric data illustrate that the salinity of type LV inclusions is lower at stage III than that at stage II (**Table 1**). One possible inference is that another fluid with lower salinity was mixed into the fluid system (Liao et al., 2014). Pressure transformed from lithostatic to hydrostatic to generate hydrothermal convection cells where meteoric waters were introduced and mixed with magmatic fluids (Chappuis et al., 2020). When ore-bearing fluids with higher temperature, salinity, and pressure as well as lower density converged with groundwater with lower temperature, salinity, and pressure, the chemical balance of the ore-forming solution was destroyed to promote the precipitation of ore minerals (Zhang, 1997). This study has shown that the depths of the

stratabound ores mainly ranged from 0.8 to 3.6 km (**Table 1; Figure 10**). Shen and Huang (1987) claimed that atmospheric water or syngenic water in sedimentary rock can mix with hydrothermal solution from magma in fault zones to form ore deposits. This mixing increased oxygen fugacity and pH value, which is favorable for the precipitation of cassiterite (Zhang, 1997). The mixing of the fluid should have had a certain relationship with stratabound ores in the Gejiu ore field (**Figure 2**).

### Roles of Boron and Fluorine in Mineralization

Both tourmaline and fluorite are widespread in all stages of the giant Gejiu Sn-Cu polymetallic mineralization. B and F played an important role in the mineralization of the giant Sn-Cu polymetallic deposit in Gejiu. Boron and fluorine appeared usually in the altered mineralization zone as tourmaline and fluorite, respectively (**Figure 3**). The addition of B led to an increase in  $\text{H}_2\text{O}$  in the melt (Pichavant, 1981). No evidence shows that  $\text{H}_2\text{O}$  increased in F-rich fluid systems (Manning, 1981). Therefore for similar degrees of fractionation and crystallization, boron-bearing magmas should have maintained a higher  $\text{H}_2\text{O}$  content than F-bearing magmas. In the boron-bearing system, the magmatic aqueous fluid phase was rich mainly in silica and sodium and poor in aluminum, whereas it was rich in aluminum in fluorine-bearing systems (Pollard et al., 1987). There were marked differences in the partition between boron and fluorine. Fluorine was partitioned toward the melting phase while boron toward the vapor phase. Consequently, B was gradually extracted from the crystallizing magmas and accumulated in fluids to form tourmaline-rich pegmatite (Ogorodova et al., 2004). The fluorine flowed to the fluids



from the crystallizing magmas only during the final stages of crystallization (Pollard et al., 1987) to form fluorite-tourmaline-chalcopyrite veins in the altered granites (Figure 3). Tin mineralization is commonly associated with the metasomatism of alkalis, including albitization, K feldspathization, greisenization, tourmalinization, chloritization, and topazization (Pollard et al., 1987). Boron was available in large amounts in the hydrothermal stage, and formed stockwork ores associated with the mineralization of magmatic-hydrothermal Sn (Figure 3F). Enrichment in F or B may be critical to the formation of the giant Gejiu Sn-Cu ore deposit. The composition of the host rock also played a role in the precipitation of tourmaline, fluorite, and cassiterite. For example, carbonate rocks acted as host rock for the mineralization of tin, and a wide variety of skarn deposits dominated the giant Gejiu Sn-Cu polymetallic deposit.

In conclusion, the ore-forming mechanism of the Gejiu Sn-Cu polymetallic deposit can be attributed mainly to the boiling and immiscibility of the ore-forming fluid with decreasing pressure and temperature, as well as the mixing of different source fluids. The continuous convective circulation of the ore-forming hydrothermal fluid solution, driven by the powerful thermal driving force of magma, promoted the accumulation of ore-forming matter and, finally, the giant Sn-Cu polymetallic deposit was formed in the Gejiu district.

## CONCLUSION

The conclusions of this study are as follows:

- (a) The ore-forming process of the giant Gejiu Sn-Cu polymetallic ore deposit can be divided into four stages: (I) skarnization; (II) greisenization; (III) cassiterite-sulfide;

- and (IV) cassiterite-tourmaline-quartz. Four types of fluid inclusions—liquid-rich aqueous (LV), vapor-rich aqueous (VL), solid-bearing (S), and aqueous-carbonic (C) inclusions were recognized in the four stages.
- (b) Fluid inclusions in the skarn stage trapped a single-phase aqueous fluid with an average salinity of 5.87–31.29 wt% NaCl at temperatures of 343–562°C, under pressures of 117–148 MPa, corresponding to the depth of 7.0–8.2 km. In the greisen stage, the fluid with an average salinity ranged from 9.43–28.46 wt% NaCl in the near-critical state, and separated into coexisting liquid and vapor phases that ascended, and were depressurized and cooled at temperatures of 284–536°C, under pressures of 84–136 MPa, corresponding to the depth of 5.50–7.75 km. In the cassiterite-sulfidation stage, the mixing of the magmatic fluid and meteoric water and the boiling and immiscibility of the fluids with decreasing in pressure and temperature are key factors to precipitation accumulation of ore minerals. Its average salinity varied from 2.53 to 25.15 wt% NaCl. The fluid cooled at temperatures of 136–482°C, under pressures of 56–101 MPa, corresponding to the depth of 4.0–6.24 km. In the cassiterite-tourmaline-quartz stage, relatively small inclusions occurred in the alteration and ore minerals. Its average salinity varied from 3.46 to 4.01 wt% NaCl. The fluid cooled at temperatures of 136–217°C, under pressures of 30–45 MPa, corresponding to the depth of 3.0–4.5 km, which may illustrate that the stage of epithermal mineralization had nearly finished.
- (c) Boron and fluorine played an important role during the mineralizations of tin and copper, respectively. The boiling, immiscibility, and mixing of the ore-forming solutions might have been crucial mechanisms in the formation of the giant Gejiu Sn-Cu polymetallic ore deposit.

## DATA AVAILABILITY STATEMENT

The original contributions presented in the study are included in the article/**Supplementary Material**, further inquiries can be directed to the corresponding author.

## AUTHOR CONTRIBUTIONS

Data curation, JL; formal analysis, ZW; funding acquisition, YC; investigation, YC; project administration, YC; supervision, YC; writing—original draft, YC; writing—review and editing, YC; All authors have read and agreed to the published version of the article.

## FUNDING

This research was funded by the National Natural Science Foundation of China (Grant Nos. 41972312, 41672329), the National Key Research and Development Project of China

## REFERENCES

- Audat, A., Güther, D., and Heinrich, C. A. (2000). Magmatic–hydrothermal Evolution in a Fractionating Granite: a Microchemical Study of the Sn–W–F–Mineralized Mole Granite (Australia). *Geochim. Cosmochim. Acta* 64, 3373–3393. doi:10.1016/s0016-7037(00)00428-2
- Bakker, R. J. (2018). AqSo\_NaCl: Computer Program to Calculate P-T-V-X Properties in the H<sub>2</sub>O–NaCl Fluid System Applied to Fluid Inclusion Research and Pore Fluid Calculation. *Comput. Geosci.* 115, 122–133. doi:10.1016/j.cageo.2018.03.003
- Bakker, R. J. (1999). *Optimal Interpretation of Microthermometrical Data from Fluid Inclusions: Thermodynamic Modelling and Computer Programming*. Heidelberg, Germany: Habilitation Thesis. University Heidelberg, 50.
- Chappuis, B. L., Christoph, A., Heinrich, C. A., Driesner, T., and Weis, P. (2020). Mechanisms and patterns of magmatic fluid transport in cooling hydrous intrusions. *Earth Planetary Sci. Lett.* 404, 304–318.
- Chen, S. Y., Zhao, P. D., Zhang, S. T., Tong, X., Wu, J. D., and Mo, G. P. (2009). Mineralizing Multiformality and Deep Prospecting of Gejiu Super Sn–Cu Multi–Metal deposit, Yunnan, China. *Earth Sci. J. China Univ. Geosci.* 34 (2), 319–324.
- Chen, Y. Q., Chen, S. Y., Huang, J. N., and Shang, Z. (2020). *Geodynamic Background–Metallogenic Process–Quantitative Evaluation of Gejiu Super–large Tin–Copper Polymetallic Deposit*. Beijing: Geological Publishing House, P206.
- Cheng, Y., Mao, J., Chang, Z., and Pirajno, F. (2013). The Origin of the World Class Tin–Polymetallic Deposits in the Gejiu District, SW China: Constraints from Metal Zoning Characteristics and 40Ar–39Ar Geochronology. *Ore Geol. Rev.* 53, 50–62. doi:10.1016/j.oregeorev.2012.12.008
- Cheng, Y., Mao, J., Rusk, B., and Yang, Z. (2012). Geology and Genesis of Kafang Cu–Sn deposit, Gejiu District, SW China. *Ore Geol. Rev.* 48, 180–196. doi:10.1016/j.oregeorev.2012.03.004
- Cheng, Y., Mao, J., Zhu, X., and Wang, Y. (2015). Iron Isotope Fractionation during Supergene Weathering Process and its Application to Constrain Ore Genesis in Gaosong deposit, Gejiu District, SW China. *Gondwana Res.* 27, 1283–1291. doi:10.1016/j.gr.2013.12.006
- Fournier, R. O. (1999). Hydrothermal Processes Related to Movement of Fluid from Plastic into Brittle Rock in the Magmatic–Epithermal Environment. *Econ. Geol.* 94, 1193–1211. doi:10.2113/gsecongeo.94.8.1193
- 308 Geological Party (1984). *Geology of Tin Deposit in Gejiu Area*. Beijing: Metallurgical Industry Publishing House. (in Chinese with English abstract).
- (Grant No. 2016YFC0600509), and the Project of China Geological Survey (Grant No. 1212011120341).

## ACKNOWLEDGMENTS

The some results of this paper were presented as a poster in SEG2017 Academic conference held at Beijing, China, September 17–20, 2017. We are particularly grateful to KuiDong Zhao (Guest Associate Editor Ryan Mathur), and two reviewers (John Leslie Walshe and Guoguang Wang) for their constructive comments and suggestions.

## SUPPLEMENTARY MATERIAL

The Supplementary Material for this article can be found online at: <https://www.frontiersin.org/articles/10.3389/feart.2021.655777/full#supplementary-material>

- Guo, J., Zhang, R. Q., Li, C. Y., Sun, W. D., Hua, Y. B., Kang, D. M., et al. (2018). Genesis of the Gaosong Sn–Cu deposit, Gejiu district, SW China: constraints from in situ LA–ICP–MS cassiterite U–Pb dating and trace element fingerprinting. *Ore Geol. Rev.* 92, 627–642.
- Hedenquist, J. W., Arribas, A., and Reynolds, T. J. (1998). Evolution of an Intrusion–Centered Hydrothermal System; Far Southeast–Lepanto Porphyry and Epithermal Cu–Au Deposits, Philippines. *Econ. Geol.* 93, 373–404. doi:10.2113/gsecongeo.93.4.373
- Henley, R. W., and McNabb, A. (1978). Magmatic Vapor Plumes and Ground–Water Interaction in Porphyry Copper Emplacement. *Econ. Geol.* 73, 1–20. doi:10.2113/gsecongeo.73.1.1
- Kesler, S. E., and Wilkinson, B. H. (2009). Resources of Gold in Phanerozoic Epithermal Deposits. *Econ. Geol.* 104, 623–633. doi:10.2113/gsecongeo.104.5.623
- Kesler, S. E., and Wilkinson, B. H. (2006). The Role of Exhumation in the Temporal Distribution of Ore Deposits. *Econ. Geol.* 101, 919–922. doi:10.2113/gsecongeo.101.5.919
- Liao, S., Chen, S., Deng, X., Li, P., Zhao, J., and Liao, R. (2014). Fluid Inclusion Characteristics and Geological Significance of the Xi’ao Copper–Tin Polymetallic deposit in Gejiu, Yunnan Province. *J. Asian Earth Sci.* 79, 455–467. doi:10.1016/j.jseae.2013.10.023
- Linnen, R. L. (1998). Depth of Emplacement, Fluid Provenance and Metallogeny in Granitic Terranes: a Comparison of Western Thailand with Other Tin Belts. *Mineralium Deposita* 33, 461–476. doi:10.1007/s001260050163
- Logan, M. A. V. (2000). Mineralogy and Geochemistry of the Gualilán Skarn deposit in the Precordillera of Western Argentina. *Ore Geol. Rev.* 17, 113–138. doi:10.1016/s0169-1368(00)00009-3
- Lu, H.-Z., Liu, Y., Wang, C., Xu, Y., and Li, H. (2003). Mineralization and Fluid Inclusion Study of the Shizhuyuan W–Sn–Bi–Mo–F Skarn Deposit, Hunan Province, China. *Econ. Geol.* 98, 955–974. doi:10.2113/gsecongeo.98.5.955
- Luo, J. L. (1995). Metallogenic Model of Tin–Tungsten–Zinc–Silver deposit in Southeast Yunnan. *Yunnan Geol.* 14 (4), 319–332. (in Chinese).
- Manning, D. A. C. (1981). The Effect of Fluorine on Liquidus Phase Relationships in the System Qz–Ab–Or with Excess Water at 1 Kb. *Contr. Mineral. Petrol.* 76, 206–215. doi:10.1007/bf00371960
- Mao, J. W., Cheng, Y. B., and Guo, C. L. (2008). Gejiu Tin Polymetallic Ore–Field: deposit Model and Discussion. *Acta Geol. Sin.* 81, 1456–1468. (in Chinese with English abstract).
- Meinert, L. D., Dipple, G. M., and Nicolescu, S. (2005). 100th Anniversary Special Paper: World Skarn Deposits. *Econ. Geol.* 100, 299–336.

- Meinert, L. D., Hedenquist, J. W., Satoh, H., and Matsuhisa, Y. (2003). Formation of Anhydrous and Hydrous Skarn in Cu-Au Ore Deposits by Magmatic Fluids. *Econ. Geol.* 98, 147–156. doi:10.2113/gsecongeo.98.1.147
- Mlnlu, F., and Kwak, T. A. P. (1994). Geology, Geochemistry, and Fluid Inclusions of the Gejiu Tin-Polymetallic Field, People's Republic of China. *Int. Geol. Rev.* 36, 272–292. doi:10.1080/00206819409465461
- Ogorodova, L. P., Melchakova, L. V., Kiseleva, I. A., and Peretyazhko, I. S. (2004). Thermodynamics of Natural Tourmaline-Elbaite. *Thermochim. Acta* 419, 211–214. doi:10.1016/j.tca.2003.12.019
- Peng, C. D. (1985). Discussion on the Mineralizing Condition and the Type Model of the Tin Deposits in Gejiu District. *Yunnan Geology* 4, 17–32. (in Chinese with English abstract).
- Pichavant, M. (1981). An Experimental Study of the Effect of boron on a Water Saturated Haplogranite at 1 Kbar Vapour Pressure. *Contr. Mineral. Petrol.* 76, 430–439. doi:10.1007/bf00371485
- Pollard, P. J., Pichavant, M., and Charoy, B. (1987). Contrasting Evolution of Fluorine- and boron-rich Tin Systems. *Mineral. Deposita* 22, 315–321. doi:10.1007/bf00204525
- Prokofev, V. Y., and Pek, A. A. (2015). Problems in Estimation of the Formation Depth of Hydrothermal Deposits by Data on Pressure of Mineralizing Fluids. *Geol. Ore deposits* 57 (1), 1–20. doi:10.1134/s1075701515010043
- Roedder, E. (1992). Fluid Inclusion Evidence for Immiscibility in Magmatic Differentiation. *Geochim. Cosmochim. Acta* 56, 5–20. doi:10.1016/0016-7037(92)90113-w
- Rusk, B. G., Reed, M. H., and Dilles, J. H. (2008). Fluid Inclusion Evidence for Magmatic-Hydrothermal Fluid Evolution in the Porphyry Copper-Molybdenum Deposit at Butte, Montana. *Econ. Geol.* 103, 307–334. doi:10.2113/gsecongeo.103.2.307
- Shao, J. L., and Mei, J. M. (1986). On the Study of Typomorphic Characteristics of mineral Inclusion in the Gold Deposits from Volcanic Terrain in Zhejiang and its Significance and Prospecting Significance. *Miner. Rocks* 6 (3), 103–111. (in Chinese with English abstract).
- Shen, W. Z., and Huang, Y. S. (1987). *Stable Isotope Geology*. Beijing: Atomic Energy Press.
- Shepherd, T. J., Rankin, A. H., and Alderton, D. H. M. (1985). *A Practical Guide to Fluid Inclusion Studies*. Blackie: Chapman & Hall.
- Sibson, R. H. (2001). Seismogenic Framework for Hydrothermal Transport and Ore Deposition. *Rev. Econ. Geol.* 14, 25–50. doi:10.5382/rev.14.02
- Sibson, R. H. (2004). Controls on Maximum Fluid Overpressure Defining Conditions for Mesozonal Mineralisation. *J. Struct. Geol.* 26, 1127–1136. doi:10.1016/j.jsg.2003.11.003
- Wilkinson, J. J. (2001). Fluid Inclusions in Hydrothermal Ore Deposits. *Lithos* 55, 229–272. doi:10.1016/s0024-4937(00)00047-5
- Zhang, D. H. (1997). Some New Advances in Ore-Forming Fluid Geochemistry on Boiling and Mixing of Fluids during the Processes of Hydrothermal Deposits. *Adv. Earth Sci.* 12 (6), 546–552.
- Zhang, J., Mao, J. W., Cheng, Y. B., and Li, X. L. (2012). Mineralization Process of the Kafang Tin-Copper deposit in the Gejiu District, Yunnan Province: Constraints from Fluid Inclusion. *Acta Petrol. Sin.* 28, 166–182. (in Chinese with English abstract).
- Zhang, S. T., Xia, Q. L., Zhao, P. D., and Gao, Y. (2008). Diversity of Mineralization and Spectrum of the Gejiu Superlarge Tin-Copper Polymetallic Deposit, Yunnan, China. *J. China Univ. Geosci.* 19 (4), 363–370. doi:10.1016/s1002-0705(08)60069-2
- Zhou, T., Yuan, F., Yue, S., Liu, X., Zhang, X., and Fan, Y. (2007). Geochemistry and Evolution of Ore-Forming Fluids of the Yueshan Cu-Au Skarn- and Vein-type Deposits, Anhui Province, South China. *Ore Geol. Rev.* 31, 279–303. doi:10.1016/j.oregeorev.2005.03.016
- Zhuang, Y. Q., Wang, R. Z., and Yang, S. P. (1996). *Tin-Copper Polymetallic Deposits*. Beijing: Earthquake Publishing House, 327. (in Chinese).

**Conflict of Interest:** The authors declare that the research was conducted in the absence of any commercial or financial relationships that could be construed as a potential conflict of interest.

Copyright © 2021 Chen, Wang and Li. This is an open-access article distributed under the terms of the Creative Commons Attribution License (CC BY). The use, distribution or reproduction in other forums is permitted, provided the original author(s) and the copyright owner(s) are credited and that the original publication in this journal is cited, in accordance with accepted academic practice. No use, distribution or reproduction is permitted which does not comply with these terms.